One serious limitation of the present study was the lack of precision navigation for either the submersible or the surface ship and the lack of subbottom profiler records precisely located with respect to the submersible traverses.

BRUCE C. HEEZEN
MICHAEL RAWSON
Lamont-Doherty Geological Observatory of Columbia University, Palisades, New York 10964

References and Notes

1. The Mariana Trench, a recognized subduction zone, was the site of the first descent by man to the ocean's greatest depths [J. Piccard and R. S. Dietz, *Seven Miles Down* (Putnam, New York, 1961)]. The Puerto Rico and Japan trenches were later explored with the bathyscaphe *Archimède* [G. Bellaiche, *C. R. Acad. Sci.* **265**, 1160 (1967); J. M. Peres, *Deep-Sea Res.* **12**, 883 (1965)]. These observers noted fresh unstable talus slopes as evidence of contemporary deformation. However, they did not relate their observations either to the then rather novel subduction process or to older structural models.
2. P. Molnar and L. R. Sykes, *Bull. Geol. Soc. Am.* **80**, 1639 (1969).
3. D. E. Karig and G. F. Sharman, *ibid.* **86**, 377 (1976).
4. W. J. Ludwig, J. Ewing, M. Ewing, S. Murauchi, N. Den, S. Asano, H. Hotta, M. Hayakawa, T. Asanuma, K. Ichikawa, I. Noguchi, *J. Geophys. Res.* **71**, 2121 (1966); J. Ewing and M. Ewing, *ibid.* **67**, 4729 (1962).
5. D. W. Scholl, R. Von Huene, J. B. Ridlon, *Science* **159**, 869 (1968).
6. D. R. Seely, P. R. Vail, G. G. Walton, in *The Geology of Continental Margins*, C. A. Burk and C. L. Drake, Eds. (Springer-Verlag. New York, 1974), pp. 249–260.
7. R. L. Fisher, *Bull. Geol. Soc. Am.* **72**, 703 (1961).
8. B. C. Heezen and M. Rawson, *Mar. Geol.* **23**, 173 (1977).
9. D. J. Fornari, A. Malahoff, B. C. Heezen, *Bull. Geol. Soc. Am.*, in press.
10. This research is supported by the U.S. Navy Office of Naval Research under contract N00014-76-C-0264. We gratefully acknowledge the cooperation of the officers and men of DSV *Turtle* and others of the U.S. Navy Submarine Development Group One. The illustrations were done by Suzanne MacDonald. Lamont-Doherty Geological Observatory Contribution 2488.

24 September 1976; revised 17 December 1976

Laser Interferometer Measurement of Changes in Crayfish Axon Diameter Concurrent with Action Potential

Abstract. *Small rapid changes in the diameter of an axon take place when an action potential progresses along the axon. In the giant axon of the crayfish these occur within a period of about 1 millisecond and are typically about 18 angstroms in total amplitude.*

Previous studies have shown that there are slow mechanical changes in nervous tissue in conjunction with an action potential (*1–4*). We have observed that when an action potential travels along an axon, the outer surface of the axon undergoes a displacement time pattern that transpires within a few milliseconds. These motions are fundamentally different from those previously observed in single cells during the course of an action potential in the algae *Nitella* and *Chara* (*2, 4*). Such motions occur over periods of seconds rather than milliseconds.

We used a laser interferometer to measure axon boundary movement accompanying the action potential in the medial giant axon of the crayfish *Procambarus clarkii*. The optical layout of the interferometer is shown in Fig. 1a. It is similar to that described by Eberhardt and Andrews (*5*), but it has a special optic fiber in the target path and features a phase-locked detection scheme developed at Stanford (*6*) which has a sensitivity only 6 db lower than that of a homodyne system and is simpler than FM detection for measurement of transients.

The optic fiber is a graded-index fiber wave guide manufactured by Corning Glass Works. It consists of a core about 80 μm in diameter surrounded by another layer of glass, bringing the total diameter of the fiber to approximately 150 μm. Its useful property for our purpose is that the core, which carries most of the light, preserves the spatial coherence of the light because its index of refraction decreases approximately parabolically with increasing radius (*7*).

Light from the target is reflected through the optic fiber back into the photodetector, where it is mixed with light from the reference beam that has been downshifted in frequency by 40 Mhz at the Bragg cell. If the target motion is given by $x(t)$, the phase shift in the returning beam is given by

$$\phi(t) = \frac{4\pi n x(t)}{\lambda}$$

where λ is the wavelength of He-Ne light (6328 Å) and n is the index of refraction of the target medium (1.33 for water). The current from the square-law photodetector contains a component at the difference frequency of the two beams (*8*)

$$i \sim \cos[2\pi f t + \phi(t) + \phi_0]$$

where f is the "carrier" frequency (40 Mhz) and ϕ_0 is the quasi-static phase due to the path length difference between the target and the reference.

To detect the phase modulation $\phi(t)$, the signal is converted to a 100-khz carrier and then multiplied by a reference sinusoid that is 90° out of phase with the

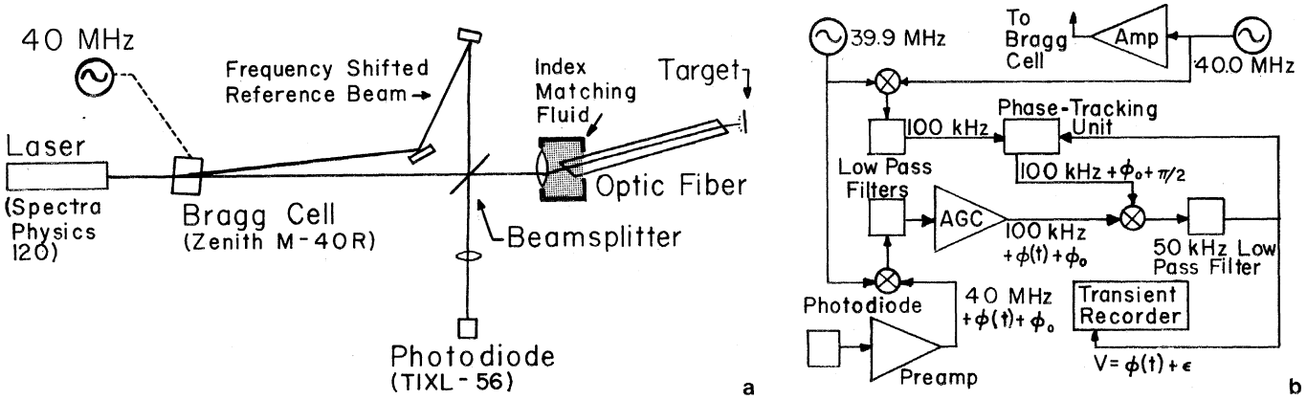

Fig. 1. Interferometer measuring system. (a) Optical system: the Bragg cell is an acousto-optic modulator, which shifts the frequency of part of the incoming light by 40 Mhz and deflects it away from the unshifted (target) beam. The photodetector is an avalanche photodiode. (b) Signal detection system: the phases of the signal and reference sinusoid are indicated at various stages of processing. The 40-Mhz carrier is converted to 100 khz so that the digital phase shifter in the phase-tracking unit need not perform at radio frequency. The automatic gain control (*AGC*) maintains the carrier at an amplitude of 10 volts to the final multiplier, so the detected phase modulation will not vary with shifts in carrier level from the photodetector. The detected output contains a d-c term ϵ, which appears if the reference sinusoid to the final multiplier shifts away from quadrature with the carrier; this voltage functions as an error signal to the feedback system.

carrier (Fig. 1b). This operation yields a signal that is directly proportional to $x(t)$ for amplitudes $\lesssim 100$ Å (*9*). The 90° phase difference is maintained by a feedback system that incorporates a digital phase shifter to correct the phase of the reference sinusoid. For these measurements, the system was set to compensate for changes with time periods greater than about 20 msec. The interferometer is capable of measuring subangstrom displacements by the use of suitable signal averaging.

The medial giant axon of *P. clarkii* is about 180 μm in diameter. A segment between the brain and the sixth ganglion was sutured at both ends, isolated by teasing away the smaller axons adhering to it, and removed from the animal. The segment, about 2 cm long, was placed in the paraffin chamber shown in Fig. 2. The electrode configuration in the chamber was designed to permit velocity measurement of both action potential and mechanical events. Platinum stimulating and recording electrodes embedded in the paraffin were spaced with the recording pair about 5 mm from the stimulating pair and the intrapair spacing about 1 mm. The axon was placed across these electrodes and stimulated with a rectangular pulse 75 μsec wide, and of sufficient amplitude (about 1 volt) to produce an action potential measured across the recording electrodes.

Throughout preparation, the nerve remained immersed in a bath of crayfish physiological solution similar to van Harreveld's (*10*). This was also true during measurement, since the optic fiber probe is designed to operate in a water medium.

For the measurement reported here, light reflection from the axon was increased by placing a small fleck of gold dust on the axon as it lay in solution. The fleck consisted of a cluster of particles of average size 3 μm, covering an irregularly shaped surface about 20 μm wide. With a micrometer positioner, the axon was placed so that the axon surface covered by the gold was approximately 50 μm from the end of the optic fiber and formed the target area. The gold reflector alleviates two problems: (i) the nearly transparent axon does not reflect enough light to yield a strong electrical signal at the detector, and (ii) the optical properties of the axon itself change during passage of the action potential (*1*, pp. 378–394).

The electrical signal was extracted from photodetector noise through signal-locked averaging of a 25-msec segment beginning 0.6 msec before the delivery of each stimulus pulse. For the measurements shown here, 1400 responses were synchronously summed and normalized to produce a relatively noise-free tracing that corresponds to the average response for a single stimulus.

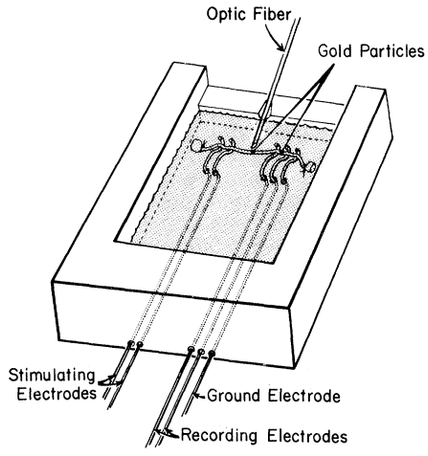

Fig. 2. Recording chamber showing nerve placement.

The pattern of the recorded motion of a typical preparation is shown in Fig. 3. The size of the total motion recorded varied from 3 to 25 Å in different preparations and was observed to decrease as a nerve was deteriorating. Slow changes, which have been shown to occur and to have a cumulative effect over the course of many stimuli (*1*, pp. 397–398), are not detected by the apparatus.

To verify that the changes observed were changes in axon diameter, gold was placed on the axon surface farthest from the probe. As predicted, with the light being reflected from the remote surface of the axon, the tracing was the inverse of that shown in the middle of Fig. 3.

To ascertain that the motion recorded was directly linked to the action potential, the amplitude of the stimulating pulse was reduced to 90 percent of threshold (the lowest stimulating voltage that will produce an action potential). With the same summing and averaging, no evidence of motion was seen, and these recordings were indistinguishable from those with no electrical stimulation. We have not explored whether, with much larger averaging, some evidence of greatly reduced motion would emerge in the absence of an action potential. In any event, the rather radical change in measured amplitude with a small change in stimulating voltage strongly links the observed motion to the existence of the action potential.

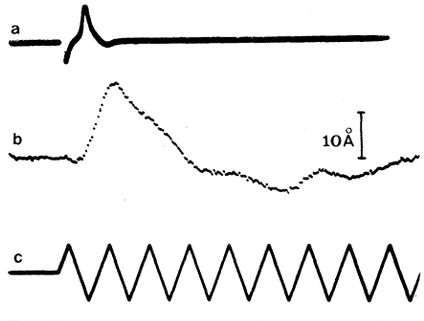

Fig. 3. (a) Action potential as measured between a single recording electrode and ground. The peak is about 1 mv. (b) Displacement pattern measured by the interferometer. A contraction, indicated by the upward trace, is seen starting about 250 μsec after stimulation and peaking about 400 μsec later. This is followed by a return to normal size, a slow expansion, and finally the return to the prestimulation diameter. (c) Time marker with a 500-μsec period. The triangle wave begins at the onset of stimulation.

If the threshold voltage is restored and the optic fiber is moved to a point 0.9 mm farther from the stimulating electrodes than it was for the recording of Fig. 3, the pattern observed is similar but displaced about 50 μsec farther along the time line. Apparently the velocity of the mechanical event moving along the axon in this preparation was about 18 m/sec. (Because the peak is not sharply defined, the error of measurement is about ± 15 percent.) A comparable measurement of the separation of the electrical peaks from the two recording electrodes (see Fig. 2) indicates the same velocity for the action potential.

Our original interest in these motions was generated by the possibility of mechanical concomitants of neural events in the cochlea. We know now that the cochlea in its most sensitive frequency range responds to displacement amplitudes much less than 1 Å. The events shown here are of the appropriate time period and of sufficient amplitude to constitute signal-synchronous concomitants of an input signal to the cochlea. Whether the mechanical events produced by the much smaller axons of the eighth nerve are correspondingly smaller than these, or differ in time course, can be determined only by much more refined techniques than those described here.

However, it does seem clear from these measurements that there are minute displacements of the axon surface closely associated with the passage of the action potential. Whether these movements are of precisely the form shown here is open to some question. What we have given is the typical result from a number of attempts. Occasionally the form of the motion has differed significantly from that shown here. Nevertheless, it does appear that with further stabilization of the axon preparation, it will be possible to manipulate the environment and the state of the axon in

ways that will eventually establish the relations between these events and the better known electrical sequence.

BRUCE C. HILL
EARL D. SCHUBERT, MARK A. NOKES
Hearing and Speech Sciences, Stanford University School of Medicine, Stanford, California 94305
ROBIN P. MICHELSON
University of California Medical Center, San Francisco 94122

References and Notes

1. L. B. Cohen, *Physiol. Rev.* **53**, 373 (1973).
2. P. H. Barry, *J. Membr. Biol.* **3**, 313 (1970); D. S. Fensom, *Can. J. Bot.* **44**, 1432 (1966).
3. L. P. Kayushin and R. G. Ludkovskaya. *Dokl. Akad. Nauk SSSR* **95**, 253 (1954); *ibid.* **102**, 727 (1955).
4. U. Kishimoto and T. Ohkawa, *Plant Cell Physiol.* **7**, 493 (1966); R. Sandlin, L. Lerman, W. Barry, I. Tasaki, *Nature (London)* **217**, 575 (1968).
5. F. J. Eberhardt and F. A. Andrews, *J. Acoust. Soc. Am.* **48**, 603 (1970).
6. B. C. Hill, thesis, Stanford University (1977); M. A. Nokes, thesis, Stanford University (1977).
7. S. Kawakami and J. Nishizawa, *IEEE Trans. Microwave Theory Tech.* **MTT-16**, 814 (1968).
8. The electric fields of the reference (R) and target (T) beams at the photodiode are given by

$$\bar{E}_R\cos[(\omega - 2\pi f_0)t + \phi_R]$$

and

$$\bar{E}_T\cos[\omega t + \phi(t) + \phi_T]$$

where ω is the optical frequency and f_0 is the Bragg cell frequency (40 Mhz). The photocurrent is proportional to the intensity

$$i \sim E_R^2 + E_T^2 + 2\,\bar{E}_R \cdot \bar{E}_T$$
$$\cos[(\omega - 2\pi f_0)t + \phi_R]\cos[\omega t + \phi(t) + \phi_T]$$

Neglecting the d-c terms $E^2_R + E^2_T$ and the terms at 2ω, we have

$$i \sim \bar{E}_R \cdot \bar{E}_T\cos[2\pi f_0 t + \phi(t) + \phi_T - \phi_R]$$

Defining $\phi_0 = \phi_T = \phi_R$ yields the expression given in the text.
9. The reference sinusoid is given by

$$V_{ref}\,(\text{volts}) = 10\cos(2\pi f_1 t + \phi_0 + \pi/2)$$

The signal is

$$V_{sig} = 10\cos[2\pi f_1 t + \phi(t) + \phi_0]$$

and $f_1 = 100$ khz. The multiplier gives an output

$$V_{out} = V_{ref}V_{sig}/10$$

Hence

$$V_{out} = 10\,\{\cos[\phi(t) - \pi/2]$$
$$+ \cos[4\pi f_1 t + 2\phi_0 + \phi(t) + \pi/2]\}/2$$

The term at $2f_1$ (200 khz) is removed by the 50-khz low-pass filter shown in Fig. 1b, leaving

$$V_{out} = 5\cos[\phi(t) - \pi/2]$$
$$= 5\sin[\phi(t)]$$
$$\simeq 5\phi(t)$$

For amplitudes in water ≤ 100 Å, V_{out} is proportional to the amplitude within 1.2 percent; at 200 Å the error is 5 percent. If $x(t) = x_0\sin(\omega_s t)$, the spectrum of the output is given by

$$V_{out} = 10 \sum_{\substack{k=1 \\ k\ \text{odd}}}^{\infty} J_k\left(\frac{4\pi n x_0}{\lambda}\right)\sin(k\omega_s t)$$

where J_k is the Bessel function of order k. This expression is analogous to the Bessel function expansion for sinusoids [H. A. Deferrari, R. A. Darby, F. A. Andrews, *J. Acoust. Soc. Am.* **42**, 982 (1967); S. M. Khanna, J. Tonndorf, W. W. Walcott, *ibid.* **44**, 1555 (1968); P. R. Dragsten, J. A. Paton, R. R. Capranica, W. W. Webb, *ibid.* **60**, 665 (1976)].
10. A. van Harreveld, *Proc. Soc. Exp. Biol. Med.* **34**, 428 (1936).

23 August 1976; revised 12 November 1976

Elemental Sulfur: Accumulation in Different Species of Fungi

Abstract. *Sulfur, in elemental form, is present in several fungi especially in self-inhibited and resting structures such as dormant spores and sclerotia. The possible importance of sulfur in fungal spore dormancy is discussed.*

Pezet and Pont have shown that elemental sulfur (S_8) is responsible for self-inhibition in *Phomopsis viticola* Sacc., that is, the failure of the alpha spores to germinate (*1*). Recently, elemental sulfur was discovered in sporocarps of the ectomycorrhizal fungus *Pisolithus tinctorius* (*2*). Several self-inhibitory mechanisms have been described for different fungi (*3*) and the problem of dormancy of fungal structures has been discussed by several investigators (*4*, *5*), but free sulfur has never been implicated in self-inhibition or spore dormancy. Dormancy of fungal spores is widespread and presumably plays an important role in evolution (*6*). Dormant spores have a reduced metabolic activity. They are thus more resistant to external unfavorable factors such as drying, high temperatures, and other deleterious environmental influences. If no dormant stage were present, germination would take place and the potential of the fungus for multiplication or dispersal would be reduced (*7*). We report here on an examination of several dormant or self-inhibited structures of different fungi, from Myxomycetes to Basidiomycetes, for the presence of elemental sulfur.

Information on fungal origin, culture media, and the particular fungal struc-

Table 1. Results of tests for the presence of elemental sulfur in different species of fungi. Medium 1 consisted of 20g of Tryptone, 3 g of yeast extract, 20 g of glucose, 4 g of KH_2PO_4, 1.2 g of $CaCl_2 \cdot 2H_2O$, 1.2 g of $MgSO_4 \cdot 7H_2O$, 0.12 g of $FeCl_2 \cdot 4H_2O$, 0.17 g of $MnCl_2 \cdot 4H_2O$, 0.07 g of $ZnSO_4 \cdot 7H_2O$, 7 g of citric acid, 0.5 mg of hemin chloride per milliliter of medium in 1 percent NaOH, 2 percent agar, and 2000 ml of water (*p*H adjusted to 4.6). Medium 2 consisted of 2 percent agar in water. Medium 3 consisted of 2 percent malt extract and 2 percent agar in water. Reactions were as follows: +, positive; −, negative.

Genus or species	Medium or natural substrate	Structures tested	Method of analysis	
			TLC	H_2S
Physarum polycephalum	Medium 1	Sclerotia	+	+
Spongospora subterranea	Potato tubers	Spore balls	+	+
Albugo candida	Shepherd's purse	Sporangia	+	+
Pythium ultimum	Medium 2	Oogonia	+	+
Botrytis cinerea	Medium 3	Conidia	+	+
Botrytis cinerea	Medium 3	Sclerotia	+	+
Erysiphe convolvulii	Leaves of small bindweed	Perithecia	−	−
Podosphaera leucotricha	Leaves of apple trees	Oidia	+	+
Gnomonia comari	Medium 3	Sporulating pycnidia	+	+
Pestalozzia sp.	Medium 3	Sporulating acervuli	+	+
Nectria cinnabarina	Deadwood	Stromata	+	+
Cytospora sp.	Medium 3	Sporulating pycnidia	+	+
Sclerotinia sclerotiorum	Medium 3	Sclerotia	+	+
Phomopsis viticola	Medium 3	Sporulating pycnidia	+	+
Phomopsis sclerotioides	Medium 3	Sclerotia and pycnidia	+	+
Monilia fructigena	Medium 3	Microconidia	+	+
Diatrype sp.	Medium 3	Perithecia	+	+
Eutypa armeniacae	Medium 3	Sporulating pycnidia	+	+
Claviceps purpurea	Rye	Ergot (sclerotia)	+	+
Melanconis sp.	Shoots of grapevine	Perithecia	+	+
Coniella diplodiella	Medium 3	Sporulating pycnidia	+	+
Septoria nodorum	Sterilized wheat	Sporulating pycnidia	+	+
Neurospora crassa	Medium 3	Conidia	+	+
Neurospora crassa (fluffy)	Medium 3	Microconidia	−	−
Gliocladium roseum	Medium 3	Conidia	+	+
Trichoderma viride	Medium 3	Conidia	+	+
Rhizoctonia solani	Medium 3	Sclerotia	+	+
Typhula ishikariensis	Sterilized wheat	Sclerotia	+	+
Ustilago hordei	Barley	Chlamydospores	+	+
Tilletia caries	Wheat	Chlamydospores	+	+
Puccinia graminis	Barberry	Aeciospores	+	+
Gymnosporangium juniperi	Pine	Teliospores	−	−
Schizophyllum commune	Medium 3	Sporocarps and basidiospores	+	+
Agaricus bisporus	Commercial fungi	Young sporocarps	−	−